2012

Numerical simulation of buoyancy-driven turbulent ventilation in attic space under winter conditions

Shimin Wang
University of Nebraska-Lincoln, swang19@unl.edu

Zhigang Shen
University of Nebraska-Lincoln, shen@unl.edu

Linxia Gu
University of Nebraska-Lincoln, gul@fit.edu

Published in *Energy and Buildings* 47 (2012), pp. 360–368; doi:10.1016/j.enbuild.2011.12.012

Submitted August 11, 2011; revised October 13, 2011; accepted December 10, 2011.

Numerical simulation of buoyancy-driven turbulent ventilation in attic space under winter conditions

Shimin Wang,[1] Zhigang Shen,[1] and Linxia Gu [2]

1. Durham School of Architectural Engineering and Construction, University of Nebraska-Lincoln, NE 68588, USA
2. Department of Mechanical and Materials Engineering, University of Nebraska-Lincoln, NE 68588, USA
Corresponding author — Z. Shen, tel 402 472-9470, fax 402 472-4087, email zshen3@unl.edu

Abstract
Attic design and construction have significant impacts on residential buildings' energy performance. In order to understand how passive ventilation rates affect ridge-vent attic's performance, a twodimensional steady-state finite volume model is employed to simulate the buoyancy-driven turbulent ventilation and heat transfer in a triangular attic space of a gable-roof residential building under winter conditions. The modeled attic has a pitch of 5/12 and a passive ventilation system, consisting of continuous ridge and soffit vents. The v2f model is used to analyze the turbulent air flow and natural convection heat transfer inside the attic. The effects of ambient air temperature, vent size, and ceiling insulation on heating load and ice dam formation are investigated. The thermal performance of the vented attic is compared with a sealed attic as well. The simulation results reveal that symmetrical air flow patterns exist in a vented attic, in contrast to the asymmetrical air flow patterns found in a sealed attic. In addition, it is suggested that increasing vent size results in higher ventilation air flow rate but barely affects the attic heating load, and that both sufficient ventilation and insulation are needed to ensure the proper functions of the attic and its energy efficiency.

Keywords: attic, ventilation, insulation, heating load, ice dam, turbulence, CFD

1. Introduction

Attic ventilation has been a prevailing practice in roof construction in the United States since 1940s [1]. For decades, the ASHRAE Handbook-Fundamentals has included recommendations for attic ventilation in residential roof construction, in order to (i) minimize condensation on the underside of roof sheathing, (ii) cool attic air during summer time, (iii) prevent ice dams during winter time, and (iv) extend the service life of the roof materials [2]. Almost all the existing building codes across the United States (e.g., the BOCA National Building Code, International Building Code, Standard Building Code, and Uniform Building Code) require attic spaces to be ventilated. Typically, the net free vent area (unobstructed area where air can freely flow from outside to inside to outside) is required to be 1/150 of the floor area of the attic space being ventilated, and a reduction of the ventilation ratio from 1/150 to 1/300 is allowed only if at least 50% of the ventilating area is in the upper portion of the space and a continuous vapor retarder is installed on the warm side of the ceiling in cold climates [3].

Despite these long-established guidelines for attic ventilation in residential building construction and retrofit, the technical data used to derive these ventilation requirements are very limited [2]. Recent research (e.g., [2,4]) has suggested that the advantages and disadvantages of providing attic ventilation need to be evaluated on a case-by-case basis, i.e., ventilation should be treated as a design option instead of a universal requirement.

The objective of this paper is to quantitatively investigate the impact of attic ventilation rates and ceiling insulation types on the attic performances of gable-roof houses, and to provide technical data for future guidelines. The focus of the paper is to employ a computational fluid dynamics (CFD) model to study the turbulent air flow and heat transfer in both sealed and vented attics.

The majority of the previous research on heat transfer in attic spaces is concerned with natural convection in triangular enclosures, as reviewed by Kamiyo et al. [5]. While a considerable number of experimental and numerical studies (e.g., [6–15]) have been devoted to the analysis of flow and heat transfer under laminar conditions, only a few studies (e.g., [16,17]) investigated turbulent flow and heat transfer. For realistic sizes of residential attics, the air flow is almost always in the turbulent regime.

Air flow and heat transfer in vented attic spaces have been scarcely investigated in the past. Medina et al. [18,19] developed a transient model for residential attics based on empirical heat transfer correlations and reported that the cumulative difference between the model predictions and experimental data was less than 12%. However, in this correlation-based model, neither air flow velocity nor temperature distribution in the attic space was solved. Moujaes and Alsaiegh [20] developed a two-dimensional steady-state finite element model to

Nomenclature

c_p	specific heat, J kg^{-1} K^{-1}
f	elliptic relaxation function
g	gravitational acceleration, m s^{-2}
h_c	heat transfer coefficient at ceiling, W m^{-2} K^{-1}
h_r	heat transfer coefficient at roof, W m^{-2} K^{-1}
k	turbulence kinetic energy, m^2 s^{-2}
L	turbulence length scale, m
p	pressure, N m^{-2}
p_{atm}	atmospheric pressure, N m^{-2}
S	strain rate, s^{-1}
t_r	roof thickness, m
T	temperature, K
T_0	reference temperature, K
T_{cb}	temperature at ceiling-bottom, K
Trt	temperature at roof-top, K
T_{in}	inlet air temperature, K
u	velocity component, m/s
$\overline{v^2}$	turbulence velocity variance scale, m^2 s^{-2}
x,y	coordinates, m

Greek symbols

β	thermal expansion coefficient, K^{-1}
ε	turbulence dissipation rate, m^2 s^{-3}
λ	thermal conductivity, W m^{-1} K^{-1}
λ_r	roof thermal conductivity, W m^{-1} K^{-1}
μ	molecular viscosity, kg m^{-1} s^{-1}
μ_t	eddy viscosity, kg m^{-1} s^{-1}
ρ	density, kg m^{-3}
σ_k	effective turbulence Prandtl number for k
σ_ε	effective turbulence Prandtl number for ε
σ_T	ffective turbulence Prandtl number for T
τ	turbulence time scale, s

simulate the thermal effects of placing a radiant barrier system inside a vented residential attic for a summer weather condition in Las Vegas. They employed the k–ε model to approximate the turbulent flow and heat transfer, and found that the use of attic radiant barrier system can reduce the ceiling cooling load by 25–30%. In their study, inlet air velocity was specified to vary between 0.2 m/s and 0.3 m/s, accounting for both the stack effect (air movement driven by buoyancy) and the wind effect, while the individual contribution of the stack effect was not isolated. In addition, the soffit vents of 10 cm and the ridge vent of 40 cm assumed in the model (corresponding to a ventilation ratio of 1/13) seem to be much larger than those adopted in the realistic buildings per building codes.

In this paper, a two-dimensional steady-state finite volume model is employed to simulate the buoyancy-driven turbulent ventilation and heat transfer in a triangular attic space of a gable-roof residential building under winter conditions. The turbulent air flow and natural convection heat transfer inside the attic is modeled in terms of the v2f model [21–23]. The v2f model is an eddy-viscosity model similar to the standard k–ε model, but incorporates nearwall turbulence anisotropy and non-local pressure-strain effects. It is a general low-Reynolds number turbulence model that is valid all the way up to solid walls, and therefore does not need to make use of wall functions. Previous studies (e.g., [24–26]) have shown that the v2f model performs the best among the Reynolds-averaged Navier–Stokes (RANS) models for indoor air flow simulations. In terms of the CFD model, the impacts of ambient air temperature, vent size, and ceiling insulation on heating load and ice dam formation will be investigated in detail. The thermal performance of the vented attic will be compared with a sealed attic as well.

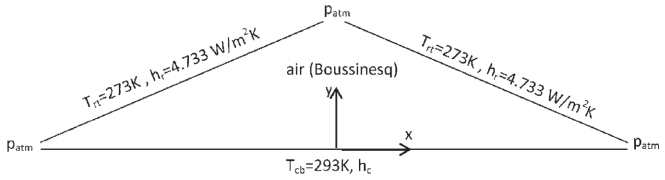

Figure 1. Schematic of the computational domain and boundary conditions.

2. Numerical model

A schematic diagram of a cross-section plan of the physical model is shown in Figure 1. In the direction perpendicular to the cross-section shown in Figure 1, it is assumed that the building is long enough to ignore the effects of the gable walls, and thus the problem can be simplified to two-dimensional. The modeled attic space has a ceiling width of 8 m and a pitch of 5/12, corresponding to a pitch angle of 22.62°. For simplicity, no trusses have been included in the model, and the computational domain is only occupied by air. Furthermore, the air is assumed to be a Boussinesq fluid with a reference temperature that is always specified to the outside ambient air temperature to correctly calculate the buoyancy effects.

In order to correctly account for the thermal resistances of the ceiling and roofs, which are excluded from the computational domain, convection-type boundary conditions are applied to both the roof and ceiling boundaries. For example, energy balance across the roof thickness gives

$$\lambda \frac{\partial T}{\partial y} = \frac{\lambda_r}{t_r}(T - T_{rt}) = h_r(T - T_{rt}) \tag{1}$$

where T_{rt} is the temperature at the roof-top, and the heat transfer coefficient h_r is the reciprocal of the roof thermal resistance.

In this study, a roof-top temperature of 273 K and a heat transfer coefficient of 4.73 W/m2 K are specified to the roof boundaries to simulate a condition of a 3 cm plywood roof covered by snow. For investigating ice dam formation, which is a major objective of this study, a fixed roof-top temperature of 273 K is a reasonable approximation to the real situation, due to the large latent heat related to ice melting or water solidification. It should be noted that in cold climates, the roof-top temperature could be much lower than 273 K, even covered by snow, but that is not the case studied here. Similarly, a ceiling-bottom temperature of 293 K and a heat transfer coefficient depending on ceiling insulation are specified to the ceiling boundary. The ceiling insulation, expressed by the R-value, is a parameter that is allowed to assume different values for different investigated cases.

The vent size and inlet air temperature are two other parameters that are allowed to vary for different cases, in addition to the ceiling insulation. For all the cases investigated in this study, balanced vent areas are assumed, i.e., the left soffit vent has the same size as the right soffit vent, and the ridge vent has an area equal to the sum of the soffit vents. Pressures at the soffit and ridge vents are all specified to be zero gauge pressure and no velocities are specified in the model. Therefore, the obtained air flow is purely driven by the thermally induced buoyancy forces, i.e., the stack effect.

Following the Reynolds-averaged approaches to turbulence, all of the unsteadiness is averaged out, i.e., all unsteadiness is regarded as part of the turbulence [27]. As a result, the time-averaged air velocity, pressure, and temperature distributions in the attic space shown in Figure 1 are governed by

the following steady-state continuity, momentum, and energy equations:

$$\frac{\partial}{\partial x_i}(\rho u_i) = 0 \tag{2}$$

$$\frac{\partial}{\partial x_j}(\rho u_i u_j) = -\frac{\partial p}{\partial x_i} + \frac{\partial}{\partial x_j}[(\mu + \mu_t)S_{ij}] - \rho g_i \beta (T - T_0) \tag{3}$$

$$\frac{\partial}{\partial x_i}(\rho c_p T u_i) = \frac{\partial}{\partial x_j}\left[\left(\lambda + \frac{c_p \mu_t}{\sigma_T}\right)\frac{\partial T}{\partial x_j}\right] \tag{4}$$

According to the v2f model [21–23], the eddy viscosity, μ_t, is defined by

$$\mu_t = C_\mu \rho \overline{v^2} \tau \tag{5}$$

and determined from the following transport equations for the turbulence kinetic energy, dissipation rate, velocity variance scale, and elliptic relaxation function:

$$\frac{\partial}{\partial x_i}(\rho k u_i) = P - \rho\varepsilon + \frac{\partial}{\partial x_j}\left[\left(\mu + \frac{\mu_t}{\sigma_k}\right)\frac{\partial k}{\partial x_j}\right] \tag{6}$$

$$\frac{\partial}{\partial x_i}(\rho\varepsilon u_i) = \frac{C_{\varepsilon 1}(1 + 0.045\sqrt{k/\overline{v^2}})P - C_{\varepsilon 2}\rho\varepsilon}{\tau} + \frac{\partial}{\partial x_j}\left[\left(\mu + \frac{\mu_t}{\sigma_\varepsilon}\right)\frac{\partial \varepsilon}{\partial x_j}\right] \tag{7}$$

$$\frac{\partial}{\partial x_i}(\rho \overline{v^2} u_i) = \rho k f - 6\rho \overline{v^2}\frac{\varepsilon}{k} + \frac{\partial}{\partial x_j}\left[\left(\mu + \frac{\mu_t}{\sigma_k}\right)\frac{\partial \overline{v^2}}{\partial x_j}\right] \tag{8}$$

$$f - L^2\frac{\partial^2 f}{\partial x_j^2} = (C_1 - 1)\frac{(2/3 - \overline{v^2}/k)}{\tau} + C_2\frac{P}{\rho k} + \frac{5\overline{v^2}k}{\tau} \tag{9}$$

where

$$P = 2\mu_t S_{ij} S_{ij} \tag{10}$$

$$S_{ij} = \frac{1}{2}\left(\frac{\partial u_i}{\partial x_j} + \frac{\partial u_j}{\partial x_i}\right) \tag{11}$$

and the turbulence time scale and length scale are defined by

$$\tau = \min\left[\max\left(\frac{k}{\varepsilon}, 6\sqrt{\frac{\mu}{\rho\varepsilon}}\right), \frac{\alpha}{\sqrt{3}}\frac{k^{3/2}}{\overline{v^2}C_\mu\sqrt{2S_{ij}S_{ij}}}\right] \tag{12}$$

$$L = C_L \max\left[\min\left(\frac{k^{3/2}}{\varepsilon}, \frac{k^{3/2}}{\overline{v^2}C_\mu\sqrt{6S_{ij}S_{ij}}}\right), C_\eta\left(\frac{\mu^3}{\rho^3\varepsilon}\right)^{1/4}\right] \tag{13}$$

The model constants take the following default values [21–23]:

$$\alpha = 0.6, C_1 = 1.4, C_2 = 0.3, C_{\varepsilon 1} = 1.4, C_{\varepsilon 2} = 1.9, C_\eta = 70, C_\mu = 0.22, C_L = 0.23, \sigma_T = 0.85, \sigma_k = 1, \sigma_\varepsilon = 1.3 \tag{14}$$

The governing equations formulated above are discretized with the finite volume method and solved by commercial CFD software Ansys Fluent 13.0 [28]. The SIMPLE algorithm is employed for solving the pressure and velocity coupling. The discretization of pressure is based on the PRESTO! scheme, while the QUICK scheme is adopted for all the other variables. Non-uniform quadrilateraldominant grids are employed, and the boundaries are inflated with nodes tightly clustered near the walls to ensure that the y^+ value for the first grid close to the walls is everywhere less than 1. A grid dependence test is conducted by comparing the results of a ~30,000 nodes grid with a ~70,000 nodes grid. It is shown that the difference between the two grids in the total mass flow rate and the wall heat transfer rate results is less than 2%. The modeling results presented in this paper are all based on grids consisting of about 30,000 nodes.

Since there is no comparable experimental or numerical data in the literature for convection air flow in vented attic spaces, the present numerical model is validated through two benchmark problems of turbulent natural convection in enclosures.

The first benchmark problem is turbulent natural convection in an air filled square cavity of 0.75 m high and 0.75 m wide. The side walls of the cavity are differentially heated by keeping the left wall at 50 °C and the right wall at 10 °C, resulting in a Rayleigh number of 1.58×10^9, while the cavity top and bottom are bounded by highly conducting walls. This problem has been studied both experimentally [29–31] and numerically [32–34], thus provides a good test to the present numerical model.

The modeling predictions shown in Figures 2 and 3 are obtained by specifying all the boundary temperatures in accordance with the experimental measurements [31] and employing an 80 × 80 non-uniform grid. The predicted mean velocity and temperature fields shown in Figure 2 are very similar to those measured from the experiments [29] and averaged from the large eddy simulation [32], while the predicted profiles of vertical velocity and temperature at the mid-height of the cavity agree very well with the experimental data [31], as shown in Figure 3.

The second benchmark problem adopted to validate the present model is turbulent natural convection of air confined in an isosceles triangle-shaped attic, which was originally solved by Ridouane et al. [16]. The modeled domain has a width of 5.46 m and a height of 2.73 m. A uniform temperature of 273 K is applied to the roofs, while the ceiling is kept at 293 K. The streamlines and isotherms predicted by the present model are shown in Figure 4. These results obtained based on the v2f model are in very good agreement with those given by Ridouane et al. [16], which were obtained based on a low-Reynolds number k–ε turbulence model.

3. Results and discussion

3.1. Sealed attic

Turbulent natural convection in a sealed attic is simulated first so that its results can be compared with the vented attic cases. The soffit vents are assumed to be 4 cm wide on each side, while the ridge vent is 8 cm wide. All the vents are sealed and assumed to be adiabatic, and the roof-top and ceiling-bottom temperatures are specified as shown in Figure 1. As a result, the ambient air temperature has no influence on the modeling results. The ceiling insulation is assumed to be R-20 (simulating the thermal resistance of a layer of 15 cm thick glass fiber), resulting in a heat transfer coefficient of $h_c = 0.284$ W/m^2 K.

The predicted streamlines and isotherms for the sealed attic case are shown in Figure 5(a and b), while the temperature variations along the ceiling and roof boundaries are shown by the solid lines in Figure 6. Similar to the results shown in Figure 4, the flow is asymmetric, although the geometry and boundary conditions are all symmetric about $x = 0$. The flow field is dominated by two convection cells, as shown by the streamlines. Air flow in the big cell is clockwise, while that in the small cell is counterclockwise. Both the ceiling and roof temperatures peak at around $x = -2$ m, where air in both cells is hottest and flows upward. The peak temperature along the ceiling is corresponding to a minimum heat flux, because the temperature difference across the ceiling thickness

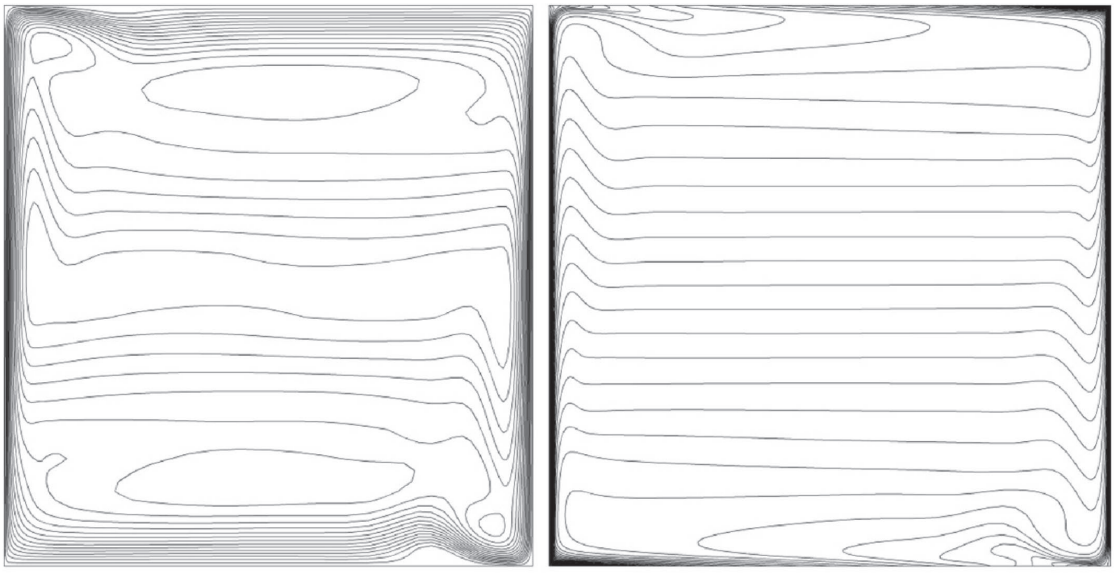

Figure 2. Predicted streamlines (a) and isotherms (b) for the validation case of turbulent natural convection in square cavity.

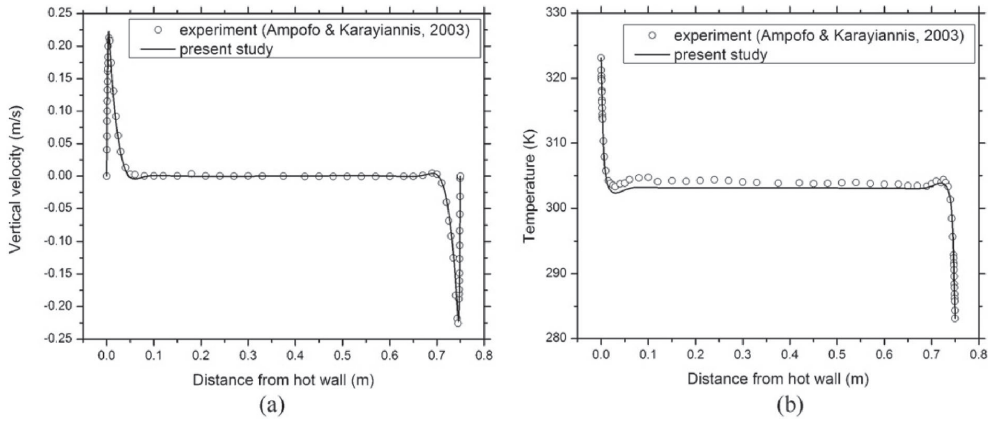

Figure 3. Comparison of predicted vertical velocity (a) and temperature (b) at mid-height of the square cavity with experimental data [31].

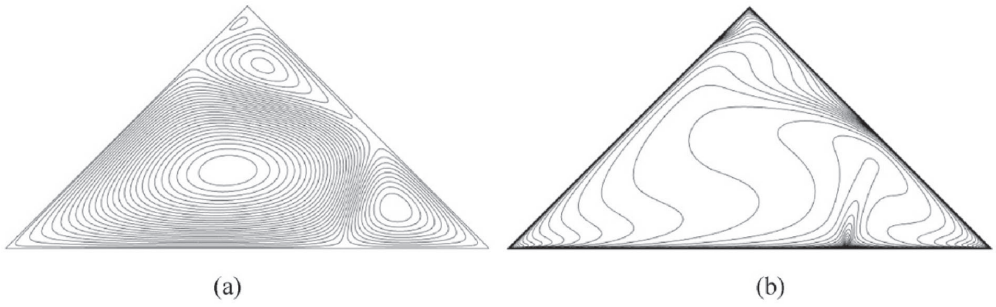

Figure 4. Predicted streamlines (a) and isotherms (b) for the validation case of turbulent natural convection in triangular cavity.

reaches the minimum there. However, the peak temperature along the roof reflects a maximum heat flux as the temperature difference across the roof thickness assumes the maximum value.

Figure 6 shows that the roof temperature for the sealed attic is everywhere above the melting point of ice, indicating a favorable condition for ice dam formation. A study by Tobiasson et al. [35] observed that severe icing problems tended to occur when the outside temperature was below 22 °F (267.5 K) and the attic air temperature was above freezing. An effective approach to avoid problematic icings is to provide appropriate attic ventilation together with sufficient ceiling insulation to maintain an attic temperature below freezing when outside is cold.

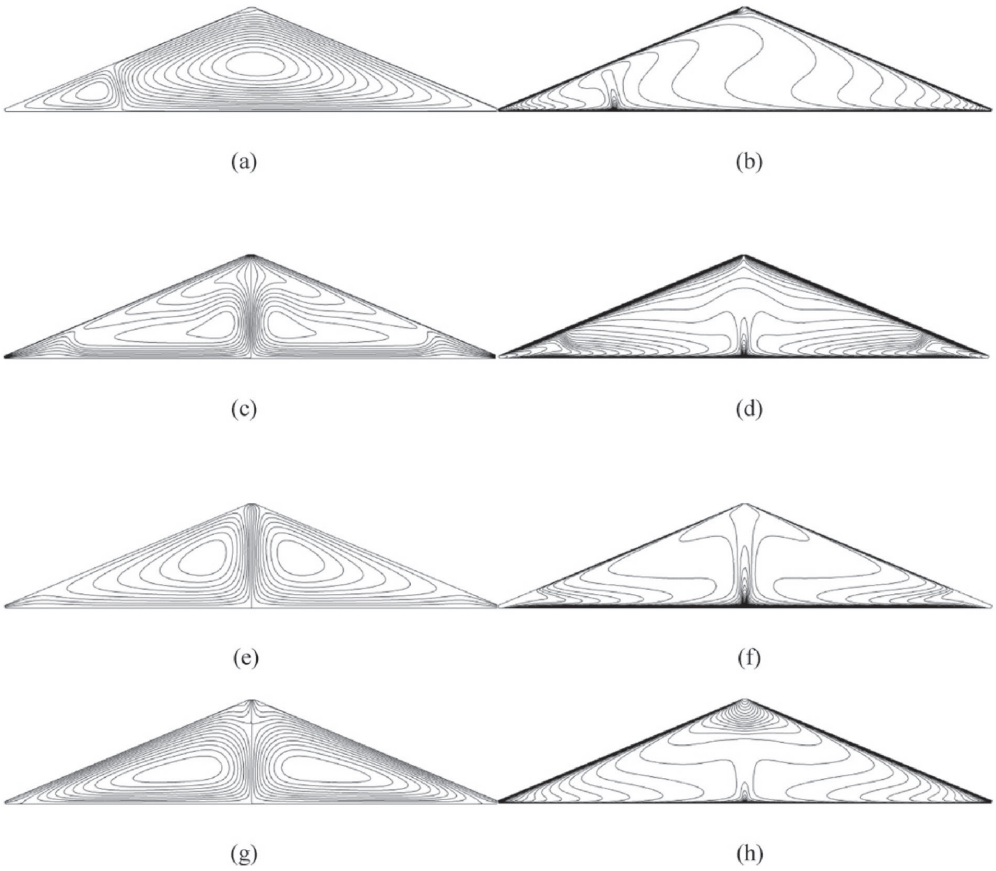

Figure 5. Predicted streamlines (left) and isotherms (right) for the cases of sealed attic (a and b), T_{in} = 263 K (c and d), T_{in} = 273 K (e and f), and T_{in} = 283 K (g and h) with 4 cm soffit vents and R-20 ceiling insulation.

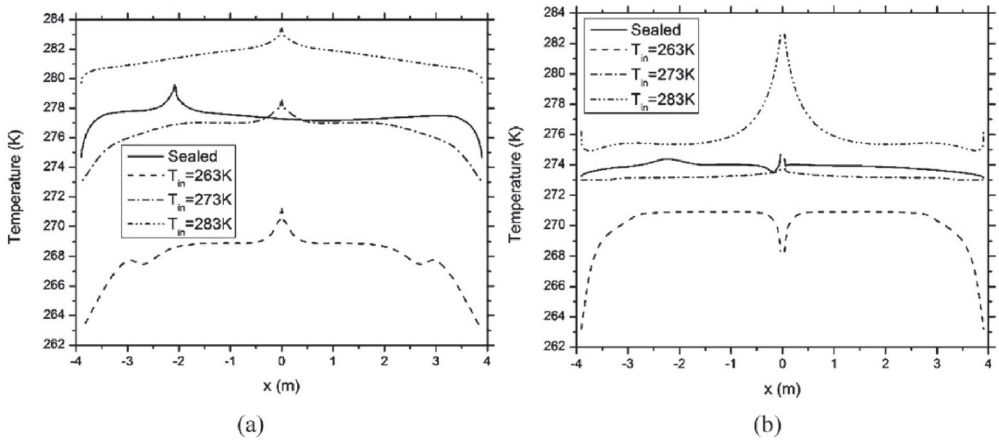

Figure 6. Predicted temperatures at the ceiling (a) and roof (b) boundaries for the cases of sealed attic, T_{in} = 263 K, T_{in} = 273 K, and T_{in} = 283 K with 4 cm soffit vents and R-20 ceiling insulation.

3.2. Effects of ambient air temperature

In contrast to the sealed attic case, the air flow and heat transfer inside a vented attic will depend on the ambient air temperature, because the outside air enters the attic at the ambient temperature. Under winter weather conditions, the ambient air temperature may be below, equal to, or above the roof temperature. These three situations are corresponding to the three cases presented below. In the modeling of these cases, a 4 cm soffit vent on each side and an 8 cm ridge vent, together with an R-20 ceiling insulation, are assumed.

In the first case, the outside air enters the soffit vents at 263 K, i.e., 10 K below the roof-top temperature. The predicted streamlines and isotherms are shown in Figure 5(c & d), while the temperature variations along the ceiling and roof boundaries are shown by the dashed lines in Figure 6. Both the velocity and temperature fields are symmetric about x = 0, which is clearly different from the asymmetric pattern for the sealed attic case. As a matter of fact, for all the vented attic cases investigated in this study, symmetric solutions are obtained. It seems that the ventilating air flow stabilizes the symmetric solution, which is unstable in the sealed attic case.

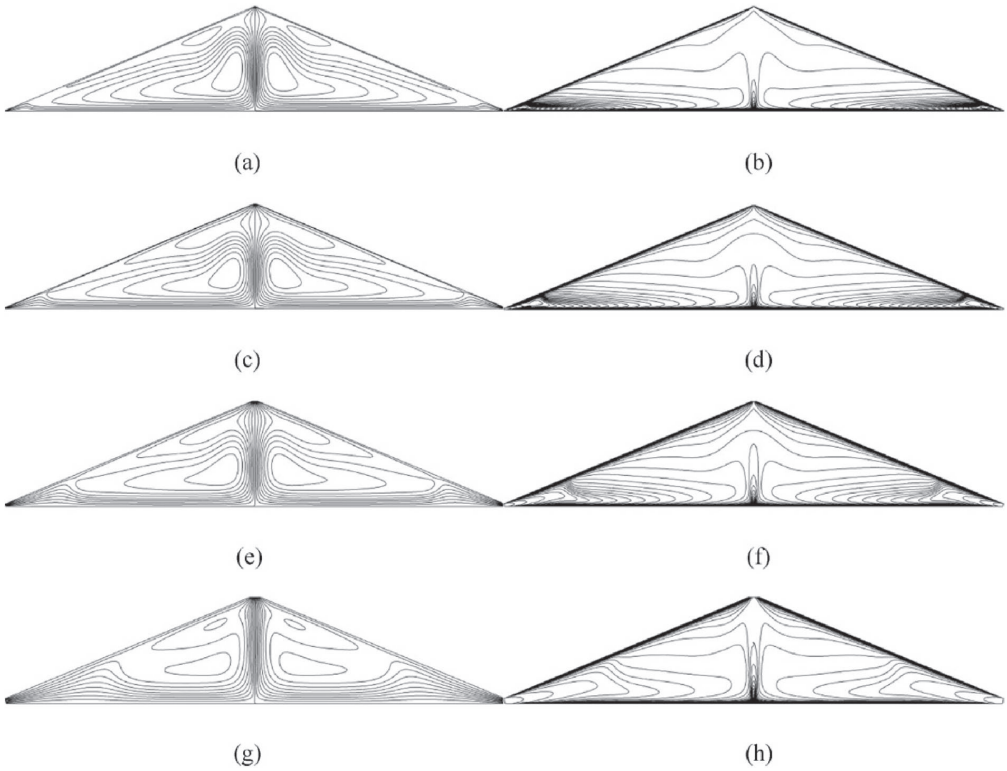

Figure 7. Predicted streamlines (left) and isotherms (right) for the cases of 1 cm (a and b), 2 cm (c and d), 4 cm (e and f), and 8 cm (g and h) soffit vents with T_{in} = 267 K and R-20 ceiling insulation.

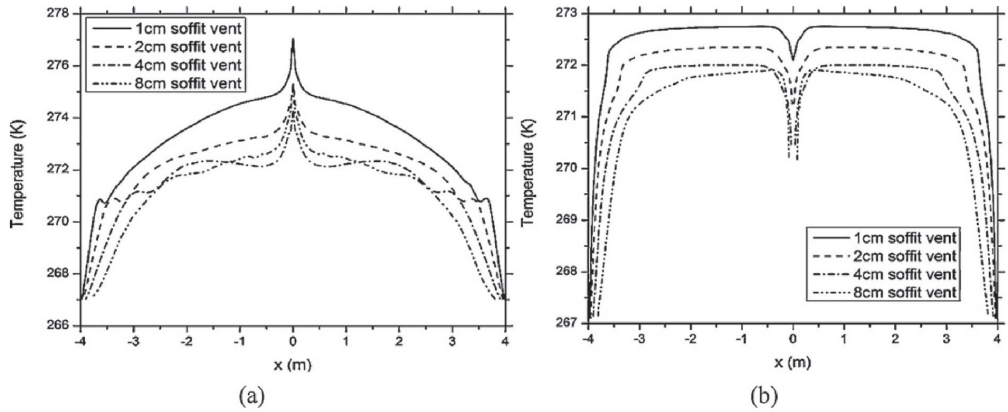

Figure 8. Predicted temperatures at the ceiling (a) and roof (b) boundaries for the cases with different vent sizes (T_{in} = 267 K and R-20 ceiling insulation).

For the T_{in} = 263 K case, since the entering air is colder than both the roof and ceiling, it is first heated from both sides near the soffit vents, then travels along the ceiling for further heating, and finally rises at the attic center and eventually leaves the attic through the ridge vent (Figure 5). The temperature distribution in the top half of the height is vertically stratified, while that in the bottom half is controlled by the two symmetric recirculating cells. The ceiling temperature peaks at the center, while the roof temperature reaches a local minimum near the ridge. Figure 6 shows that the temperature is below 271 K along the entire roof width, indicating a cold roof that will not allow ice dam to form.

In the second case of vented attic, the inlet air is assumed to have a temperature of 273 K, equal to the roof temperature. The model predictions are shown in Figure 5(e & f) and by the dash-dot lines in Figure 6. The outside air, entering from the soffit vents, is first heated along the ceiling, then forms a rising vertical plume around the attic center line, x = 0. At each side of the plume, there is a recirculating convection cell. The temperature distribution is dominated by the plume and convection cells, and no vertical stratification is observed in the temperature field. Both the ceiling and roof temperatures peak at x = 0.

In the third case, the inlet air temperature is assumed to be 283 K. The results are presented in Figure 5(g and h) and by the dash-dot-dot lines in Figure 6. Different from both the T_{in} = 263 K and T_{in} = 273 K cases, air flow in the T_{in} = 283 K case is downward, i.e., entering from the ridge vent and leaving through the soffit vents. The reason for the sinking air flow is that it is actually cooled instead of heated in the attic space. Although the inlet air could be cooled by the roofs and heated by

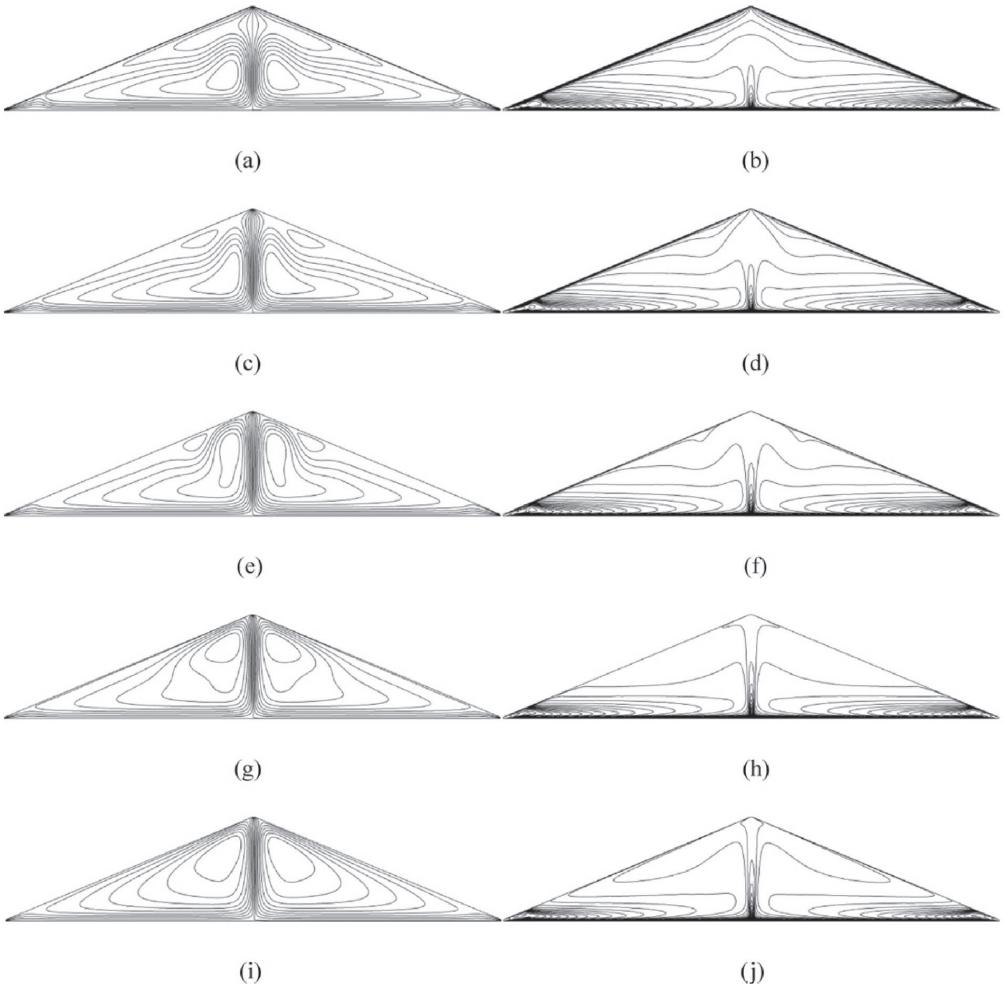

Figure 9. Predicted streamlines (left) and isotherms (right) for different ceiling insulation cases of R-20 (a & b), R-10 (c & d), R-5 (e & f), R-2.5 (g & h), and R-1.2 (i & j) with T_{in} = 267 K and 2 cm soffit vents.

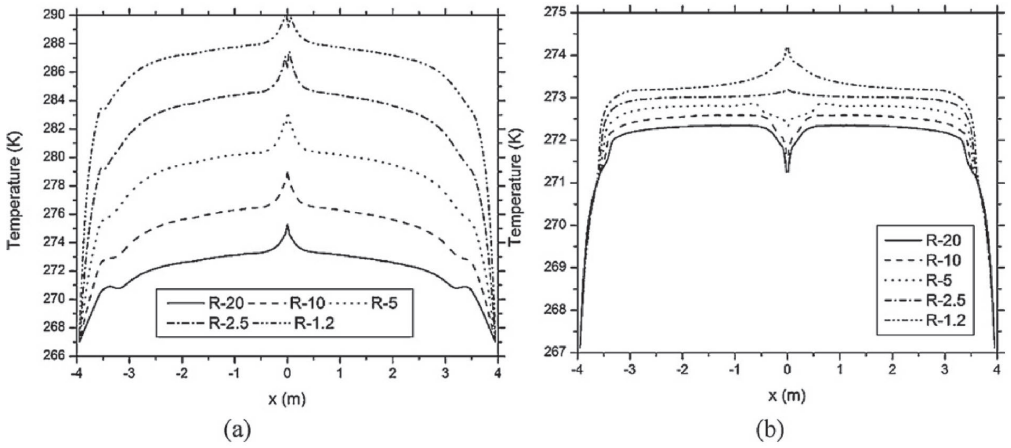

Figure 10. Predicted temperatures at the ceiling (a) and roof (b) boundaries for the cases with different ceiling insulation levels (T_{in} = 267 K and 2 cm soffit vents).

the ceiling, the much better insulation across the ceiling than that across the roofs makes the cooling effect dominate. As a result, the outside air, entering from the ridge vent, mainly travels along the roofs. Below the roof free stream sit two recirculating convection cells. The temperature field is stratified only at the top portion above the convection cells. Figure 6 shows the roof temperature is well above the ice point, but it is not relevant to ice dam formation, because the outside temperature is too high to allow ice dams to form.

The total heat transfer rates across the ceiling and roof boundaries as well as the air flow rates for the three cases with different inlet air temperatures are compared in Table 1,

Table 1. Predicted total heat transfer through the ceiling and roof boundaries and air flow rate across the attic for the cases of sealed attic, T_{in} = 263 K, T_{in} = 273 K, and T_{in} = 283 K with 4 cm soffit vents and R-20 ceiling insulation.

Inlet air temperature (K)	Heat gain from ceiling (W/m)	Heat gain from roof (W/m)	Upward mass flow rate (kg/s m)
sealed	34.4	−34.4	0
263	55.4	109.2	0.0445
273	36.6	−7.78	0.0305
283	25.6	−117.0	−0.0176

Table 2. Predicted total heat transfer through the ceiling and roof boundaries and air flow rate across the attic for the cases with different vent sizes (T_{in} = 267 K and R-20 ceiling insulation).

Soffit vent size (cm)	Ventilation rate	Heat gain from ceiling (W/m)	Heat gain from roof (W/m)	Upward mass flow rate (kg/s m)
1	1:200	44.8	21.5	0.0137
2	1:100	46.8	40.8	0.0238
4	1:50	47.7	56.8	0.0409
8	1:25	46.7	63.8	0.0675

Table 3. Predicted total heat transfer through the ceiling and roof boundaries and air flow rate across the attic for the cases with different ceiling insulation levels (T_{in} = 267 K and 2 cm soffit vents).

Ceiling insulation	Heat transfer coefficient (W/m^2 K)	Heat gain from ceiling (W/m)	Heat gain from roof (W/m)	Upward mass flow rate (kg/s m)
R-20	0.284	46.8	40.8	0.0238
R-10	0.568	81.2	32.5	0.0264
R-5	1.136	130.4	23.4	0.0292
R-2.5	2.272	188.6	13.7	0.0320
R-1.2	4.733	257.8	2.04	0.0347

together with the sealed attic case. The heat gain from the ceiling reflects the energy consumption of the attic space in the heating load of the building. Table 1 shows that a vented attic consumes more energy in cold days and saves heating energy in warm days, as compared to a sealed attic. It is also observed from Table 1 that the air flow rate in cold days is higher than that in warm days. Considering that the moisture entering an attic from the conditioned space of a building is more likely to condensate in cold days, the higher ventilation air flow rate offers a natural regulation to meet the need of venting moisture out of the building.

3.3. Effects of vent size

In this section, modeling results of attic ventilation with different vent sizes will be presented. Four sizes of soffit vent, viz., 1 cm, 2 cm, 4 cm, and 8 cm, are analyzed. For all the four cases, the size of ridge vent is kept as twice of the soffit vent to satisfy the balanced ventilation condition, and the ceiling insulation is kept as R-20. The inlet air temperature is set to 267 K, in order to investigate the possibility of ice dam formation. Based on field observations, Tobiasson et al. [35] concluded that problematic icings developed very slowly, if at all, when the outside temperature was above 267.5 K. The choice of outside temperature of 267 K is corresponding to a condition that is most favorable for ice dam development.

The predicted streamlines and isotherms are shown in Figure 7, while the ceiling and roof temperatures are shown in Figure 8. The flow and temperature fields for the different vent sizes exhibit similar pattern, although quantitative variations exist, as evident in Figure 8 and Table 2. In general, both the ceiling and roof temperatures decrease with increasing vent size, indicating larger vents bring stronger cooling effects. Figure 8 shows that the roof temperature is below 273 K for all the cases, indicating a cold roof is maintained that prevents ice dam to form.

A comparison of total heat transfer through the roofs and ceiling as well as air flow rate across the attic for different vent sizes is provided in Table 2. The table shows that the air flow rate increases with the vent size but not in a linear way. For example, the increase of the soffit vent from 1 cm to 2 cm increases the air flow rate by 71%, while the increase from 4 cm to 8 cm only increases the air flow rate by 51%. It is interesting to observe that the heat gain from the ceiling is barely influenced by the vent size change. This may be explained by that the higher mass flow rate associated with a larger vent gains more heat from the roofs, as evident from Table 2.

3.4. Effects of ceiling insulation

The effects of ceiling insulation on heating load and ice dam formation are investigated through five cases with ceiling insulation of R-20, R-10, R-5, R-2.5, and R-1.2, respectively. The attic is assumed to have a ventilation system consisting of a 2 cm soffit vent on each side and a 4 cm ridge vent, while the inlet air temperature is kept as 267 K.

As shown in Figure 9, the flow and temperature fields vary significantly with the ceiling insulation change. It can be observed that two big convection cells increase with the decrease of the ceiling thermal resistance, and eventually dominate the temperature distribution.

Figure 10 shows that both the ceiling and roof temperatures increase when ceiling thermal resistance decreases. Also shown in Figure 10 is that the roof temperatures in the R-2.5 and R-1.2 cases are higher than 273 K, favoring ice dam formation. This result provides quantitative evidence to support the qualitative common believing that a combination of appropriate attic ventilation and sufficient ceiling insulation is required to effectively prevent ice dam formation.

In Table 3, total heat transfer through the roofs and ceiling as well as air flow rate across the attic are compared for different ceiling insulation levels. Along with the decrease of ceiling thermal resistance, both heat gain from the ceiling and air flow rate increase, while the heat gain from roofs decreases. Therefore, improving the ceiling insulation not only helps preventing ice dams but also provides an effective way to reduce heating energy consumption.

4. Conclusions

Buoyancy-driven turbulent ventilation in attic space under a gable roof under winter conditions is simulated in terms of a CFD model. The findings from the numerical results are summarized as follows:

(1) For all the investigated cases, air flow in vented attics tends to be symmetric, in contrast to the asymmetric pattern found for air flow in sealed attics.
(2) As compared to a sealed attic, a vented attic consumes more energy in cold days and saves heating energy in warm days.
(3) Ventilation air flow rate is higher in cold days than in warm days, providing a natural regulation to satisfy the varying demand of venting moisture out of a building.
(4) Increasing vent size results in higher ventilation air flow rate but barely affects the attic heating load.
(5) Both sufficient ventilation and ceiling insulation are needed to effectively prevent ice dam formation and make a building energy-efficient.

It should be noted that the above-mentioned conclusions are subject to the limitations of the model assumptions adopted in this study. This research can be furthered in the

following aspects:

(1) Investigating wind effects. The air flows presented in this study are purely driven by buoyancy. Such buoyancy-driven cases are corresponding to a worst-case scenario, because real attic ventilation is generally enhanced by winds.

(2) Including moisture transfer. The contribution of the latent heat associated with moisture transfer may be significant for the energy performance of attics in humid climates, especially in summer times.

(3) Simulating attic ventilation under summer conditions. The results presented in this paper apply to winter conditions only, but the methodology employed here can be extended to investigate attic ventilation under summer conditions or year-round performance as well.

Acknowledgment — This study was partially supported by the Faculty Seed Grants from the Research Council of the University of Nebraska-Lincoln (2009–2010).

References

[1] Federal Housing Administration, *Property Standards and Minimum Construction Requirements for Dwellings*, Washington DC, 1942.

[2] W. B. Rose, A. TenWolde, Venting of attics and cathedral ceilings, *ASHRAE Journal* 44 (10) (2002) 26–33.

[3] J. I. Hutchings, *National Codes Handbook,* McGraw Hill, 1998.

[4] A. F. Rudd, J.W. Lstiburek, Vented and sealed attics in hot climates, *ASHRAE Transactions* 104 (2) (1998) 1199–1210.

[5] O. M. Kamiyo, D. Angeli, G. S. Barozzi, M. W. Collins, V.O.S. Olunloyo, S. O. Talabi, A comprehensive review of natural convection in triangular enclosures, *ASME Applied Mechanics Reviews* 63 (060801) (2010) 1–13.

[6] R. D. Flack, C. L. Witt, Velocity measurements in two natural convection air flows using a laser velocimeter, *ASME Journal of Heat Transfer* 101 (1979) 256–260.

[7] R. D. Flack, The experiment al measurement of natural convection heat transfer in triangular enclosures heated or cooled from below, *ASME Journal of Heat Transfer* 102 (1980) 770–772.

[8] D. Poulikakos, A. Bejan, Natural convection experiments in a triangular enclosure, *ASME Journal of Heat Transfer* 105 (1983) 652–655.

[9] G. A. Holtzman, R. W. Hill, K. S. Ball, Laminar natural convection in isosceles triangular enclosures heated from below and symmetrically cooled from above, *ASME Journal of Heat Transfer* 122 (2000) 485–491.

[10] H. Asan, L. Namli, Laminar natural convection in a pitched roof of triangular cross-section: summer day boundary conditions, *Energy and Buildings* 33 (2000) 69–73.

[11] E. H. Ridouane, A. Campo, M. McGarry, Numerical computation of buoyant airflows confined to attic spaces under opposing hot and cold wall conditions, *International Journal of Thermal Sciences* 44 (2005) 944–952.

[12] C. Lei, S. W. Armfield, J. C. Patterson, Unsteady natural convection in a water-filled isosceles triangular enclosure heated from below, *International Journal of Heat and Mass Transfer* 51 (2008) 2637–2650.

[13] E. F. Kent, Numerical analysis of laminar natural convection in isosceles triangular enclosures, Proceedings of the Institution of Mechanical Engineers, Part C, *Journal of Mechanical Engineering Science* 223 (2009) 1157–1169.

[14] S. C. Saha, J. C. Patterson, C. Lei, Natural convection and heat transfer in attics subject to periodic thermal forcing, *International Journal of Thermal Sciences* 49 (2010) 1899–1910.

[15] S. C. Saha, Unsteady natural convection in a triangular enclosure under isothermal heating, *Energy and Buildings* 43 (2011) 695–703.

[16] E. H. Ridouane, A. Campo, M. Hasnaoui, Turbulent natural convection in an airfilled isosceles triangular enclosure, *International Journal of Heat and Fluid Flow* 27 (2006) 476–489.

[17] S. O. Talabi, V.O.S. Olunloyo, O. M. Kamiyo, M. W. Collins, T. G. Karayiannis, Flow field and Reynolds stress distribution in low turbulence natural convection in a triangular cavity, in: K. Hanjalic, Y. Nagano, S. Jakirlic (Eds.), *Proc. Fifth International Symposium on Turbulence, Heat and Mass Transfer,* Dubrovnik, Croatia, 2006, pp. 511–514.

[18] M. A. Medina, D. L. O'Neal, W. D. Turner, A transient heat and mass transfer model of residential attics used to simulate radiant barrier retrofits, Part I: development, *ASME Journal of Solar Energy Engineering* 120 (1998) 32–38.

[19] M. A. Medina, D. L. O'Neal, W. D. Turner, A transient heat and mass transfer model of residential attics used to simulate radiant barrier retrofits, Part II: validation and simulations, *ASME Journal of Solar Energy Engineering* 120 (1998) 39–44.

[20] S. F. Moujaes, N. T. Alsaiegh, Numerical heat transfer attic model using a radiant barrier system, *Journal of Energy Engineering* 126 (2000) 32–51.

[21] P. A. Durbin, Separated flow computations with the k-ε-v^2 model, *AIAA Journal* 33 (4) (1995) 659–664.

[22] M. Behnia, S. Parneix, Y. Shabany, P. A. Durbin, Numerical study of turbulent heat transfer in confined and unconfined impinging jets, *International Journal of Heat and Fluid Flow* 20 (1999) 1–9.

[23] S. Parneix, P. A. Durbin, M. Behnia, Computation of a 3D turbulent boundary layer using the V2F model, *Flow Turbulence and Combustion* 10 (1998) 19–46.

[24] Ch. Heschl, W. Sanz, P. Klanatsky, F. Madou, Comparison of different turbulence models to compute wall affected room airflows, CFD Forum, 2005.

[25] Z. Zhang, W. Zhang, Z. Zhai, Q. Chen, Evaluation of various turbulence models in predicting airflow and turbulence in enclosed environments by CFD: Part 2–comparison with experimental data from literature, *HVAC&R Research* 13 (6) (2007) 871–886.

[26] S. M. El-Behery, M. H. Hamed, A comparative study of turbulence models performance for turbulent flow in a planar asymmetric diffuser, *World Academy of Science, Engineering and Technology* 53 (2009) 769–780.

[27] J. H. Ferziger, M. Peric, *Computational Methods for Fluid Dynamics,* 3rd ed., Springer, 2002.

[28] ANSYS FLUENT 13.0, ANSYS, Inc., Canonsburg, PA, USA, 2011.

[29] Y. S. Tian, T. G. Karayiannis, Low turbulence natural convection in an air filled square cavity, Part I: the thermal and fluid flow fields, *International Journal of Heat and Mass Transfer* 43 (2000) 849–866.

[30] Y. S. Tian, T. G. Karayiannis, Low turbulence natural convection in an air filled square cavity, Part II: the turbulence quantities, *International Journal of Heat and Mass Transfer* 43 (2000) 867–884.

[31] F. Ampofo, T. G. Karayiannis, Experimental benchmark data for turbulent natural convection in an air filled square cavity, *International Journal of Heat and Mass Transfer* 46 (2003) 3551–3572.

[32] S.-H. Peng, L. Davidson, Large eddy simulation for turbulent buoyant flow in a confined cavity, *International Journal of Heat and Fluid Flow* 22 (2001) 323–331.

[33] M. Omri, N. Galanis, Numerical analysis of turbulent buoyant flows in enclosures: Influence of grid and boundary conditions, *International Journal of Thermal Sciences* 46 (2007) 727–738.

[34] M. Omri, N. Galanis, Evaluation of confined natural and foeced convection predictions by different turbulence models, *International Journal of Numerical Methods for Heat and Fluid Flow* 19 (2009) 5–24.

[35] W. Tobiasson, J. Buska, A. Greatorex, Ventilating attics to minimize icings at eaves, *Energy and Buildings* 21 (1994) 229–234